# Predominance of hexamethylated 6-methyl branched glycerol dialkyl glycerol tetraethers in the Mariana Trench: Source and environmental implication

Wenjie Xiao[1], Yasong Wang[1], Yongsheng Liu[1], Xi Zhang[1], Linlin Shi[1], Yunping Xu[1,2*]

[1] Shanghai Engineering Research Center of Hadal Science & Technology, College of Marine Sciences, Shanghai Ocean University, Shanghai 201306, China

[2] Key Laboratory of Sustainable Exploitation of Oceanic Fisheries Resources, Ministry of Education, Shanghai Ocean University, Shanghai 201306, China

***Correspondence**. Yunping Xu (ypxu@shou.edu.cn)

**Abstract.** Branched glycerol dialkyl glycerol tetraethers (brGDGTs) are useful molecular indicators for organic carbon (OC) source and paleoenvironment. Their application in marine environments, however, is complicated because of a mixed terrestrial and marine source. Here, we examined brGDGTs in sediments from the Mariana Trench, the deepest ocean without significant terrestrial influence. Our result shows a strong predominance of hexamethylated 6-methyl brGDGT (IIIa') (73.40 ± 2.39% of total brGDGTs) and an absence of 5-methyl brGDGTs, different from previously reported soils and marine sediments that comprised both 5-methyl and 6-methyl brGDGTs. This unique feature, combined with high $\delta^{13}C_{OC}$ (–19.82 ± 0.25%), low OC/TN ratio (6.72 ± 0.84), low branched and isoprenoid tetraether (BIT) index (0.03 ± 0.01) and high acyclic hexa-/pentamethylated brGDGTs ratio (7.13 ± 0.98), support that brGDGTs in the Mariana Trench sediments are autochthonous rather than terrestrial products. The cross plot of acyclic hexa-/pentamethylated brGDGTs ratio and fractional abundance of brGDGT-IIIa' provides a novel approach to distinguish terrestrial and marine-derived brGDGTs. The compiling of literature data shows that the enhanced fractional abundance of hexamethylated 6-methyl brGDGTs is a common phenomenon in continental margins when the marine influence was intensified. Given the uniqueness of the Marina Trench, we recommend more studies for different trenches and shallow regions in order to holistically understand the biosynthesis and environmental control of brGDGTs.

## 1. Introduction

Glycerol dialkyl glycerol tetraethers (GDGTs), including isoprenoidal GDGTs (iGDGTs) and branched GDGTs (brGDGTs), are widely distributed biomarkers in terrestrial and marine settings (De Rosa and Gambacorta, 1988; Sinninghe Damsté et al., 2000). iGDGTs containing isoprenoid carbon skeleton are predominantly synthesized by archaea belonging to the phylum Thaumarchaeota (Knappy et al., 2011; Schouten et al., 2008; Sinninghe Damsté et al., 2002; Zeng et al., 2019). Unlike iGDGTs, brGDGTs consisting of 4 – 6 methyl groups and 0 – 2 cyclopentane moieties are synthesized by some bacteria including, but not limit to, Acidobacteria (Sinninghe Damsté et al., 2011). These bacteria are able to alter the degree of methylation and cyclization of brGDGTs with changing ambient environmental conditions (Weijers et al., 2007a). A survey for global soils reveals that the Cyclization of Branched Tetraethers (CBT) correlates with soil pH, while the Methylation of Branched Tetraethers (MBT) is dependent on mean annual air temperature (MAT) and to less extent on soil pH (De Jonge et al., 2014a; Weijers et al., 2007a), leading to the development of brGDGTs-based MBT/CBT proxies for pH and MAT. BrGDGTs are generally more abundant in peats and soils than marine sediments, and decrease from coastal to distal marine sediments (Hopmans et al., 2004; Schouten et al., 2013). Thus, brGDGTs and iGDGTs were thought to be biomarkers for terrestrial (particularly soil) and marine organic matter, respectively. This source difference led to the development of Branched vs. Isoprenoid Tetraether (BIT) index for estimation of terrestrial (soil) OC in marine sediments (Hopmans et al., 2004).

BrGDGTs-derived proxies such as BIT, MBT and CBT have been used to assess OC source (Herfort et al., 2006; Kim et al., 2006; Loomis et al., 2011; Wu et al., 2013), soil pH and MAT in diverse environments (Peterse et al., 2012; Sinninghe Damsté et al., 2008; Weijers et al., 2007b; Yang et al., 2014). However, one weakness of these proxies is the source uncertainty. Although brGDGTs were assumed to be specific for soil/peat bacteria (Hopmans et al., 2004; Weijers et al., 2007a,b), different compositions of brGDGT among rivers (Zell et al., 2013; Zell et al., 2014a; Zhang et al., 2012), lakes (Buckles et al., 2014; Loomis et al., 2011; Sinninghe Damsté et al., 2009; Tierney and Russell, 2009), marine waters (Liu et al., 2014; Xie et al., 2014; Zell et al., 2014b) and sediments (Peterse et al., 2009; Xiao et al., 2016; Zhu et al., 2011) suggest multiple sources. Besides temperature and pH, oxygen (Qin et al., 2015) and moisture (Dang et al., 2016a) can also influence

57 the composition of GDGTs. For example, in a Swiss lake (Lake Lugano), the vertical pattern of
58 brGDGTs and bacterial 16S rRNA gene data suggested that brGDGTs were synthesized by multiple
59 groups of bacteria thriving under contrasting redox regimes (Weber et al., 2018).
60 Weijers et al. (2007b) detected nine brGDGT isomers in peat/soils and assigned them to 5-
61 methyl brGDGTs. De Jonge et al. (2013) developed a new chromatographic method using two silica
62 columns, and found that the brGDGTs previously identified as 5-methyl brGDGTs were actually
63 mixtures of 5-methyl and 6-methyl isomers. As a result, the number of brGDGTs increased from 9
64 to 15, which was further expanded after the identification of 7-methyl brGDGTs (Ding et al., 2016).
65 The analytical improvement has opened a window for the redefinition and recalibration of
66 brGDGTs-derived proxies (De Jonge et al., 2014a; Xiao et al., 2015). Adopting the new
67 chromatographic method, several studies have provided the clues of in-situ production of brGDGTs
68 in rivers (De Jonge et al., 2014b; De Jonge et al., 2015), lakes (Weber et al., 2015; Weber et al.,
69 2018) and marine sediments (De Jonge et al., 2016; Sinninghe Damsté, 2016). However, rivers,
70 lakes and marginal seas are usually subject to terrestrial influence, making it difficult to distinguish
71 allochthonous terrestrial and autochthonous aquatic contributions to the brGDGT pool.
72 Here, we choose the Challenger Deep, Mariana Trench, to study brGDGTs in marine settings.
73 This deepest trench (11000 m) is remote from any landmass, and has no significant terrestrial
74 influence (Jamieson, 2015). Our goals are: 1) to determine the composition and concentration of
75 brGDGTs in the Mariana Trench sediments and constrain their source; and 2) to characterize in-situ
76 production of brGDGTs in marine sediments and assess their environmental implication.
77

78 **2. Material and methods**

79 **2.1 Study area and samples**

80 The Mariana Trench is formed as the subduction of Pacific plate beneath the eastern edge of
81 the Philippine Sea plate. It has a total length of ca. 2500 km and a mean width of 70 km (Fryer,
82 1996). The Challenger Deep is located in southern rim of the Mariana Trench and has the water
83 depth of 11000 m. The Mariana Trench is overlain by extremely oligotrophic waters with annual
84 primary production of 59 g C $m^{-2}$ $y^{-1}$ (Jamieson, 2015). However, sediments in the Challenger Deep
85 were found to support elevated microbial activity compared to adjacent abyssal plains (Glud et al.,

2013). This characteristic has been attributed to unique "V"-shaped geometry, intense seismic activity and high-frequency fluid dynamics within the trench that promote lateral transport of sediments and organic matter from shallow regions into the trench bottom (Jamieson, 2015; Xu et al., 2018).

During an expedition aboard RV Zhangjian (Dec. 2016 to Feb. 2017), a sediment core (MT1, 11 cm long) was retrieved from the Challenger Deep using an autonomous 11000 m-rated lander (Fig. 1). The core was immediately stored at –20 °C in a dark room until transported to the laboratory in Shanghai (China). The core was sliced at 1 – 2 cm interval. All sediment samples ($n$ = 10) were freeze dried at –40 °C and homogenized by steel spatulas.

Besides the Mariana Trench sediments, a soil sample (Soil-1) from China grassland was analyzed. This soil sample was used for comparison of brGDGTs between soil and trench sediments.

### 2.2 Lipid extraction and GDGT analyses

Sediment samples (0.5 – 2 g) were mixed with an internal standard $C_{46}$ GDGTs (Huguet et al., 2006) and 15 ml of dichloromethane/methanol (3:1, v/v). After ultrasonically extracted for 15 min, the extracts were centrifuged (3000 rpm, 5 min), and the supernatants were decanted into clean flasks. This extraction was repeated three times. The combined extracts were concentrated by a rotary evaporator and further blown down to dryness under mild nitrogen streams. The total lipid extract was dissolved in hexane/isopropanol (99:1, v/v) and filtered through a 0.45 μm PTFE filter. An Agilent ultrahigh performance liquid chromatography-atmospheric pressure chemical ionization–triple quadruple mass spectrometry system (UHPLC-APCI-MS) was used for analysis of GDGTs. The separation of 5- and 6-methyl brGDGTs was achieved with two silica LC columns in sequence (150 mm × 2.1 mm; 1.9 μm, Thermo Finnigan; USA). The detailed instrumental parameters were described by Hopmans et al. (2016). The protonated ions were $m/z$ 1050, 1048, 1046, 1036, 1034, 1032, 1022, 1020 and 1018 for brGDGTs, 1302, 1300, 1298, 1296 and 1292 for iGDGTs and 744 for $C_{46}$ GDGT. Since the response factors of GDGTs were not determined due to the lack of authentic standard, we did not calculate the absolute concentration of GDGTs. Instead, we reported the relative concentration based on peak areas (pa) of respective GDGTs normalized to total GDGTs.

115

116 **2.3 GDGT-derived parameters**

117 The BIT index, ratio of acyclic hexa- to pentamethylated brGDGTs and weighted average
118 number of cyclopentane moieties for the tetramethylated brGDGTs ($\#rings_{tetra}$) were calculated
119 according to the definitions of Hopmans et al. (2004), Xiao et al. (2016) and Sinninghe Damsté
120 (2016), respectively.

121 $$BIT = (Ia + IIa + IIIa + IIa' + IIIa')/(Ia + IIa + IIIa + IIa' + IIIa' + Cren) \quad (1)$$

122 $$\sum IIIa / \sum IIa = (IIIa + IIIa')/(IIa + IIa') \quad (2)$$

123 $$\#rings_{tetra} = (Ib + 2*Ic)/(Ia + Ib + Ic) \quad (3)$$

124 The roman numbers denote relative abundance of GDGTs that were depicted in Fig. 2.

125

126 **2.4 Bulk geochemical analysis**

127 About 1 – 2 g of each sediment sample was treated with 1 N HCl to remove carbonates, rinsed
128 with ultrapure water and then freeze-dried. After homogenized with an agate mortar and pestle,
129 approximately 35 – 40 mg of decarbonated sediments were analyzed using a model 100 isotope
130 ratio mass spectrometer (IsoPrime Corporation, Cheadle, UK) and a Vario ISOTOPE cube elemental
131 analyzer (Elementar Analysensystem GmbH, Hanau, Germany). All isotopic data were reported in
132 δ notation relative to VPDB. The intra-lab standards for normalizing stable isotopic composition of
133 OC ($\delta^{13}C_{OC}$) was USG24 (Graphite, –16.05‰) (IAEA, Vienna, Austria). The average standard
134 deviation of each measurement, determined by replicate analyses of two samples, was ±0.004 wt%
135 for organic carbon (OC) content, ±0.031 wt% for total nitrogen (TN) content and ±0.03‰ for $\delta^{13}C_{OC}$.

136

137 **2.5 Literature data compilation**

138 The dataset is composed of 2031 samples, including 634 soil samples, 473 peat samples, 88
139 river samples, 410 lake samples and 426 marine samples (Fig. 1). The sample information was listed
140 in supplementary material. The soil samples are from globally distributed soils (De Jonge et al.,
141 2014a; Ding et al., 2015; Lei et al., 2016; Li et al., 2018; Wang et al., 2016; Wang et al., 2019; Wang
142 et al., 2018; Xiao et al., 2015; Yang et al., 2015; Zang et al., 2018). The peat samples are from 96
143 different peatlands around the world (Naafs et al., 2017). The river samples are from the Danube

River (Freymond et al., 2016), the Yenisei River (De Jonge et al., 2015) and the Tagus River (Warden et al., 2016). The lake samples are from East African lakes (Russell et al., 2018), Chinese lakes (Dang et al., 2018; Dang et al., 2016b; Li et al., 2017), the Lake St Front (Martin et al., 2019), the Lake Lugano and other lakes in the European Alps (Weber et al., 2018). The marine samples are from Atlantic Ocean (Warden et al., 2016), the Kara Sea (De Jonge et al., 2016; De Jonge et al., 2015), the Berau River delta (Sinninghe Damsté, 2016), the Ceará Rise (Soelen et al., 2017), the North Sea (Dearing Crampton-flood et al., 2018), and the Mariana Trench (this study). The criteria for citing the literature data is that 5- and 6-methyl brGDGTs should be separated and quantified. It is noted that two studies (Martin et al., 2019; Weber et al., 2018) have analyzed 5-, 6- and 7-methyl brGDGTs, but due to very limited reports for 7-methyl brGDGTs, they are not included in our literature dataset.

### 2.6 Statistical analysis

The SPSS package 22 (IBM, USA) was used for statistical analyses including Pearson correlation coefficient ($r$) and one-way Analysis of Variance (ANOVA). The significance level was set at $p < 0.05$.

## 3. Results

### 3.1 Bulk geochemical parameters

The OC content, TN content, molar ratio of OC and TN content (OC/TN) and $\delta^{13}C_{OC}$ were summarized in Table 1. The OC and TN contents of sediments varied between 0.26% and 0.31% with an average of 0.28 ± 0.01% (mean ± STD; same hereafter) and between 0.04% and 0.06% (0.05 ± 0.01%), respectively. The OC/TN ratio and $\delta^{13}C_{OC}$ ranged from 5.62 to 8.34 (6.72 ± 0.84) and –19.47‰ to −20.27‰ (–19.82 ± 0.25%), respectively. Both the $\delta^{13}C_{OC}$ and OC/TN ratio were comparable to previously reported levels for the southern Mariana Trench rim and slope ($\delta^{13}C_{OC}$, –20.48 ± 0.88%; OC/TN, 7.00 ± 1.76) (Luo et al., 2017).

### 3.2 Composition and fractional abundance of GDGTs

The fractional abundance of iGDGTs and brGDGTs were summarized in Table 2. iGDGTs

were the dominant components, accounting for 96.8% to 98.6% of total GDGTs in Mariana Trench sediments. The proportion of brGDGTs was substantially lower than that of iGDGTs, ranging from 1.4% to 3.2%. For all sediment samples, the BIT index remained at a low level (0.03 ± 0.01).

With improved chromatographic performance, 5- and 6-methyl brGDGTs were completely separated (Fig. 3a,b). Interestingly, the mass chromatograms of the Mariana Trench sediment (MT-4) only showed a single peak for acyclic penta- (*m/z* 1036; Fig. 3c) and hexamethylated (*m/z* 1050; Fig. 3d) brGDGTs. This feature is different from most previous studies that two or more peaks (i.e., 5-, 6- and even 7-methyl brGDGTs) occurred in soils, lake and marine sediments (e.g., De Jonge et al., 2013; Ding et al., 2016; Xiao et al., 2015). In order to determine the structure of brGDGTs, we compared the mass spectra of brGDGTs between MT-4 and Soil-1. The soil sample (Soil-1) has been reported to contain both 5-methyl brGDGTs (major component) and 6-methyl brGDGTs (minor component) (Xiao et al., 2015), and its IIIa/IIIa' and IIa/IIa' ratios are 12.5 and 8.2, respectively (Fig. 3a, b). For the mixed sample of Soil-1 (soil) and MT-4 (Mariana Trench), the mass spectrum showed two peaks for *m/z* 1050 (hexamethylated brGDGTs) as well as for *m/z* 1036 (pentamethylated brGDGTs) (Fig. 3e, f). The comparison of retention time among Soil-1, MT-4 and the mixed sample (Soil-1 + MT-4) revealed that the peaks of *m/z* 1050 and 1036 in MT-4 were pentamethylated 6-methyl brGDGTs (IIa') and hexamethylated 6-methyl brGDGTs (IIIa'), respectively, eluting after respective 5-methyl brGDGTs (Fig. 3). This structural assignment was corroborated by an intermediate level of 5-methyl/6-methyl brGDGT ratio in the mixed sample (1.4 for *m/z* 1050 and 7.4 for *m/z* 1036) compared to that in Soil-1 (12.5 and 8.2, respectively) and MT-4 (0 for both) (Fig. 3).

In the sediment core of the Mariana Trench, the brGDGTs were constantly dominated by 6-methyl isomers (82.25 – 86.91%). The fractional abundance of 5-methyl brGDGTs, however, was too low to be quantified. BrGDGT-IIIa' was the dominant compound (73.40 ± 2.39% of total brGDGTs), followed by brGDGT-Ia (12.46 ± 1.14%) and brGDGT-IIa' (10.45 ± 1.20%). The proportion of cyclic compounds (brGDGT-Ib, Ic, IIb') was only 3.69 ± 0.75%, resulting in a low level of $\#rings_{tetra}$ (0.26 ± 0.04). The classification based on the number of methyl groups showed the dominance of hexamethylated brGDGTs (73.53 ± 2.56%) over tetramethylated (15.43 ± 1.53%) and pentamethylated (11.04 ± 1.49%) brGDGTs.

## 4. Discussion

### 4.1 In-situ production of 6-methyl brGDGTs in the Mariana Trench

To our knowledge, there are only two studies reporting GDGTs in the Mariana Trench. Guan et al. (2019) investigated iGDGT distribution in the surface sediments (4900 – 7068 m depth) from the southern Mariana Trench, while Ta et al. (2019) analyzed iGDGTs and brGDGTs in two sediment cores (*ca.* 5400 m depth) in subduction plate of the Mariana Trench. However, neither of these studies separated the 5- and 6-methyl brGDGTs. Our improved chromatographic method demonstrated the strong predominance of 6-methyl brGDGTs and the absence of 5-methyl brGDGTs in the Mariana Trench sediments. In order to decipher the mechanism of producing such unique compositions of brGDGTs, the source assessment is needed.

Multiple lines of evidence (i.e., $\delta^{13}C_{OC}$, OC/TN ratio and biomarkers) support an in-situ production of brGDGTs in the Mariana Trench. The $\delta^{13}C_{OC}$ and OC/TN ratio are widely used indicators to distinguish terrestrial vs. marine OC (Meyers, 1997). Generally, marine algae and bacteria are protein-rich and have the OC/TN ratio of 4 to 10, whereas vascular land plants are cellulose and lignin-rich and have the OC/TN ratio of 20 or greater. Due to different carbon sources and photosynthetic pathways, the typical $\delta^{13}C_{OC}$ is between *ca*. –22‰ and –20‰ for marine organisms (Meyers, 1994) and *ca*. –27‰ for terrestrial $C_3$ plants (O'Leary, 1988). Sediments from the Mariana Trench yielded high $\delta^{13}C_{OC}$ values (–19.82 ± 0.25‰) and low OC/TN ratio (6.72 ± 0.84), suggesting that sedimentary OC is of a pure marine source (Fig. 4). Thus, the terrestrial contribution to the brGDGT pool in the Mariana Trench is insignificant.

Long-distance dust transport might deliver brGDGTs from continent to open ocean. Unfortunately, there is no report about brGDGTs for eolian dust in the Mariana Trench region. Weijers et al. (2014) compared the composition of brGDGTs between marine sediments and atmospheric dust in the equatorial West African coast, and their great difference suggested an in-situ production rather than dust input for brGDGTs in the marine sediments. Here, we compared the brGDGT compositions between the Mariana Trench sediments and terrestrial samples reported in literatures (Fig. 5). Relative to the Mariana Trench sediments (brGDGT-Ia 12.46 ± 1.14%, 5-methyl brGDGTs ~0, brGDGT-IIIa' 73.40 ± 2.39%), those terrestrial samples had significantly higher

proportions of brGDGT-Ia (soil 37.52 ± 25.91%, peat 59.40 ± 21.19%, river 15.38 ± 2.97%) and 5-methyl brGDGTs (soil 23.56 ± 14.83%, peat 34.04 ± 19.18%, river 33.25 ± 8.51%), but lower proportions of brGDGT-IIIa' (soil 4.89 ± 4.82%, peat 4.86 ± 4.68%, river 11.68 ± 4.40%) ($p < 0.005$) (Fig. 5). In addition, those terrestrial samples are globally distributed, many of which are from inner Asian continent, a major source area for the dust in North Pacific (Husar et al., 2001). Thus, brGDGTs in the Mariana Trench sediments are unlikely derived from atmospheric dusts.

Low BIT index of the Mariana Trench sediments (0.03 ± 0.01; Fig. 6) is similar to distal marine sediments (an average of 0.04) (Weijers et al., 2014), again suggesting insignificant terrestrial inputs in the Mariana Trench. By compilation of globally distributed 1354 soils and 589 marine sediments, Xiao et al. (2016) proposed the (IIIa + IIIa')/(IIa + IIa') ratio as an indicator for source of brGDGTs, which was < 0.59 in 90% of soils and 0.59 – 0.92 and > 0.92 in marine sediments with and without significant terrestrial inputs, respectively. For the Mariana Trench sediments, the (IIIa + IIIa')/(IIa + IIa') ratio varied between 5.68 and 8.33 (7.13 ± 0.98) (Fig. 6). Such high (IIIa + IIIa')/(IIa + IIa') ratio suggests a predominant marine source for brGDGTs in the Mariana Trench sediments.

Overall, the bulk geochemical parameters, the composition of brGDGTs and the BIT index unanimously support the in-situ product rather than terrestrial input for brGDGTs in Mariana Trench sediments.

### 4.2 High proportion of br GDGT-IIIa' as a common phenomenon in marine environments

Not only the Mariana Trench, but also continental margins showed relatively high proportions of hexamethylated 6-methyl brGDGTs in sediments. Dearing Crampton-flood et al. (2018) investigated brGDGTs and bulk properties of organic matter in a sediment core from the North Sea Basin. The OC content, $\delta^{13}C_{OC}$ value, BIT and $\#rings_{tetra}$ index indicated a transition from the predominant marine OC in the Pliocene to the predominant terrestrial OC in the Pleistocene. Correspondingly, the proportion of brGDGT-IIIa' was significantly higher in the Pliocene (8.06 ± 1.92%) than the Pleistocene (5.16 ± 0.83%), and exhibited a significant correlation with $\delta^{13}C_{OC}$ ($R^2 = 0.68$, $p < 0.001$) and the BIT index ($R^2 = 0.46$, $p < 0.001$) (Fig. 7a, b, c). Similar to the North Sea Basin, the proportion of GDGT-IIIa' in the Kara Sea also showed a significant correlation with $\delta^{13}C_{OC}$ ($R^2 = 0.34$; $p < 0.001$) and the BIT index ($R^2 = 0.50$; $p < 0.001$) during the past 13.3 thousand

years (Fig. 7d, e, f) (De Jonge et al., 2016). These results suggest that brGDGTs synthesized by marine organisms comprise higher fractional abundance of hexamethylated 6-methyl brGDGTs.

Besides temporal variations in sediment cores, the fractional abundance of 6-methyl brGDGTs also changed from land to sea in modern samples. Warden et al. (2016) analyzed brGDGTs along a transect from the Tagus River to the deep ocean off the Portuguese margin. Along this transect, the BIT index significantly decreased from 0.9 to < 0.1, reflecting an increase in marine contribution to the sedimentary OC pool (Fig. 7h). Meanwhile, the proportion of brGDGT-IIIa' substantially increased from 11.07 ± 2.62% to 29.31 ± 6.45%, and brGDGT-IIIa' became the dominant compound of brGDGTs (Fig. 7g). In surface sediments of the Berau River delta, the $\#rings_{tetra}$ index, an indicator for source of brGDGTs, showed a marked increase from the river mouth (0.22) to the shelf break (0.83) (Sinninghe Damsté, 2016), while the proportion of brGDGT-IIIa' increased seawards, presenting similar distribution patterns as the $\delta^{13}C_{OC}$ and BIT index (Fig. 7i, j, k).

In sum, the studies for the Kara Sea (De Jonge et al., 2016), the North Sea Basin (Dearing Crampton-flood et al., 2018), the Tagus River basin (Warden et al., 2016) and the Berau River delta (Sinninghe Damsté, 2016) show enhanced fractional abundance of 6-methyl brGDGTs (particularly IIIa') as marine influence was intensified. These findings, along with the strong predominance of brGDGT-IIIa' in the Mariana Trench sediments, suggest that the high proportion of brGDGT-IIIa' in total brGDGTs is a common phenomenon in marine environments where in-situ production of brGDGTs is significant.

### 4.3 Potential mechanisms to produce high fractional abundance of brGDGT-IIIa'

A survey of brGDGTs in globally distributed soils suggested that brGDGT producing microbes could adjust their membrane lipid compositions in response to changing environmental conditions, reflected by the increase in cyclization degree of brGDGTs and the shift from 5- to 6-methyl group with increasing pH, and decreasing methylation of brGDGTs with temperature (De Jonge et al., 2014a; Ding et al., 2015; Weijers et al., 2007a; Xiao et al., 2015). This adaption mechanism may be extrapolated to marine brGDGTs producing organisms. In the Mariana Trench, in-situ production yielded brGDGTs with the strong predominance of brGDGT IIIa' (> 69%), low proportion of cyclopentane-containing brGDGTs (< 10%) and low level of the $\#rings_{tetra}$ index (< 0.32). These

289 characters seem contrast to the previous result that the fractional abundance of cyclopentane-
290 containing brGDGTs is positively correlated with pH (Sinninghe Damsté, 2016). This difference
291 can be explained by two reasons. First, the isomerization of brGDGTs is a more efficient way in
292 response to changing pH compared to the cyclization of brGDGTs (Ding et al., 2015). Based on the
293 global soil dataset, the soil pH presents stronger correlations with the Isomerization of Branched
294 Tetraethers index (IBT; Xiao et al., 2015) than with the $\#rings_{tetra}$ index as well as the cyclization
295 index ($CBT_{5me}$) (De Jonge et al., 2014a). Meanwhile, the global soils with pH > 8 ($n$ = 58) are
296 characterized by higher fractional abundance of 6-methyl brGDGTs (68.22 ± 10.41%) than the
297 cyclopentane-containing brGDGTs (16.69 ± 9.43%). Thus, weakly alkaline sediment and seawater
298 (pH ~8.0) may be an important factor for producing more 6-methyl hexamethylated brGDGTs in
299 the Mariana Trench. The second explanation is the effect of low temperature. Marine microbes tend
300 to produce more hexamethylated brGDGTs at low temperature (Sinninghe Damsté, 2016), thus
301 reducing the proportion of cyclic tetramethylated and pentamethylated brGDGTs. The ternary
302 diagram, plotted with fractional abundance of tera-, penta- and hexa-methylated brGDGTs (Fig. 8),
303 shows that brGDGTs in the Mariana Trench sediments comprise high fractional abundance of
304 hexamethylated brGDGTs (73.53 ± 2.56%). Given these facts, we propose that low temperature and
305 high pH in deep-sea environments are responsible for the production of brGDGTs with high degree
306 of methylation and predominance of 6-methyl brGDGTs, especially brGDGT-IIIa'.
307 In-situ production of brGDGTs may take place in water column, sediments, or both. Sinninghe
308 Damsté (2016) suggested that in-situ production of brGDGTs was a widespread phenomenon in
309 shelf sediments that was especially pronounced at 50 – 300 m depths. The extended dataset (63 –
310 5521 m depths) showed a large variability for the degree of cyclization of brGDGTs (Weijers et al.,
311 2014), suggesting that the brGDGTs are mainly produced in sediments where the pH of porewater
312 is more variable than that of overlying seawaters. However, in the Mariana Trench sediments, the
313 degree of cyclization fell in a narrow range (0.26 to 0.32). As a result, both water column and
314 sediments are the possible locales to produce brGDGTs.
315 The bottom of the Mariana Trench is an extreme environment, characterized by high
316 hydrostatic pressure (> 100 MPa), low temperature (*ca*. 2 °C) and darkness (Jamieson, 2015). In
317 addition, the surface waters in the Mariana Trench region are extremely oligotrophic, leading to low

sinking flux of particulate organic matter to the seafloor. Under such an extreme condition, the unique microbes may have been evolved, such as proliferation of hydrocarbon-degrading bacteria (Liu et al., 2019). These deep-sea microbes may have different response to changing ambient temperature and pH as their shallow-dwelling counterparts, and thus produce brGDGTs with different compositions. The investigations of microbial community and intact polar lipids are needed for understanding the source and environmental implication of brGDGTs in the Mariana Trench and other marine settings.

### 4.4 Deciphering brGDGT provenance in marine sediments

There are increasing concerns about the robustness of brGDGT-based proxies. Deciphering the provenance of brGDGTs is prerequisite for the application of brGDGTs-based proxies. In continental margins, intense land-sea interaction occurs, resulting in the complex composition and source of brGDGTs (De Jonge et al., 2016; Dearing Crampton-flood et al., 2018; Sinninghe Damsté, 2016). Our study highlights that marine in-situ production of brGDGTs tends to exhibit higher fractional abundance of brGDGT-IIIa' relative to terrestrial brGDGTs. However, there is an overlap for the fractional abundance of brGDGT-IIIa' between soil and marine sediments (De Jonge et al., 2014a). Xiao et al. (2016) developed the (IIIa + IIIa')/(IIa + IIa') ratio to distinguish brGDGTs from soils (< 0.59), marine sediments with terrestrial influence (0.59 – 0.92) and without terrestrial influence (> 0.92). However, some overlaps still exist between soils and marine sediments (Fig. 9). In order to circumvent this problem, we combine the (IIIa + IIIa')/(IIa + IIa') ratio and fractional abundance of brGDGT-IIIa' to evaluate the source of brGDGTs (Fig. 9). Specifically, the cross plot of (IIIa + IIIa')/(IIa + IIa') ratio and fractional abundance of brGDGT-IIIa' reveals that the slope of global soils (30.5 ± 0.7) is significantly larger than that of marine sediments with terrestrial influence (8.2 ± 0.1), and both are significantly larger than the slope of the Mariana Trench sediments without significant terrestrial influence (2.3 ± 0.3) (Fig. 9).

The unique composition of brGDGTs in the Mariana Trench has significant implications on the brGDGTs-based proxies. As a remote setting from the landmass, the Mariana Trench provides an opportunity to distinguish marine in situ production from a terrestrial origin of brGDGTs that usually muddles the interpretation of shelf sediments. However, it is unclear what the similarity and

difference are for brGDGTs-producing microbes and their response to environmental factors between the Mariana Trench and continental shelf. In addition, the weight contribution to the brGDGT pool from sediments and water column remains elusive. Since factors such as nutrients, particle loading, bacterial community, and oceanographic parameters (e.g., oxygenation, salinity, currents) vary significantly between the shelf and trench as well as among different hadal trenches, the brGDGT-producing microbes are likely different. Therefore, the investigation of brGDGTs in multiple hadal trenches and shallow marine regions are needed to decipher their source and environmental control, that are beneficial for accurate application of the brGDGTs-based proxies such as MBT, CBT and BIT.

## 5. Conclusions

Our study represents the first investigation for 5-methyl and 6-methyl brGDGTs in the hadal trench, enabling us to draw four conclusions.

1) The Mariana Trench sediments are characterized by the strong predominance of 6-methyl brGDGTs (84.57 ± 1.53% of total brGDGTs), especially brGDGT-IIIa' (73.40 ± 2.39%), whereas 5-methyl brGDGTs are below detection limit. This unique feature has been never reported and attributed to the combined effect of insignificant terrestrial influence, alkaline seawater and low subsurface temperature in the Mariana Trench.

2) High brGDGT (IIIa + IIIa')/(IIa + IIa') ratios (7.13 ± 0.98), enriched $\delta^{13}C_{OC}$ signatures (–19.82 ± 0.25%), low OC/TN ratios (6.72 ± 0.84), low BIT index (0.03 ± 0.01), high abundance of 6-methyl brGDGTs and absence of 5-methyl brGDGTs support an in-situ production of brGDGTs in the Mariana Trench sediments.

3) BrGDGTs in sediments from the Mariana Trench and continental margins comprise higher proportion of hexamethylated 6-methyl brGDGTs with intensified marine influence. The slope of fractional abundance of brGDGT-IIIa' and the (IIIa + IIIa')/(IIa + IIa') index can be used to decipher terrestrial and marine provenance of brGDGTs. Since in-situ production of predominant hexamethylated 6-methyl brGDGTs influences the robustness of brGDGT-based proxies, this study provides a new way to estimate brGDGT sources and holds some promise in reducing uncertainty of brGDGTs-based paleoenvironmental proxies.

4) The uniqueness of the Mariana Trench that is remote from any landmass allows distinguishing marine in situ production from a terrestrial origin of brGDGTs. However, it is unclear how comparable this unique site is to shallow marine settings and other hadal trenches. Therefore, the comparison studies of brGDGTs for different hadal trenches as well as between hadal and non-hadal sites are recommended.

***Data availability***. Data have been made available through FIGSHARE: https://doi.org/10.6084/m9.figshare.9896120.v1 (Xiao et al., 2019)

***Author contributions***. WX and YX developed the study design. Field work for this study was conducted by YX. WX, YW, YL, XZ and LS conducted the experiments and data analyses. All authors contributed to data interpretation. WX and YX compiled and processed all presented data and wrote the manuscript.

***Competing interests***. The authors declare that they have no conflict of interest.

***Acknowledgements.*** Samples were obtained during cruises by the RV Zhangjian. We are grateful to captains and crews for their excellent support to obtain the samples. Drs. Weicheng Cui, Binbin Pan and Jiasong Fang are thanked for assistance in sampling and GDGT analysis. The cruise is financially supported by the Shanghai Committee of Science and Technology (15DZ1207000). The additional financial supports are from National Natural Science Foundation of China (41976030; 41676058), State Key Laboratory of Marine Geology, Tongji University (No. MGK202003), and Qingdao National Laboratory for Marine Science and Technology (QNLM2016ORP0208). Two anonymous reviewers and associate editor (Prof. Silvio Pantoja) are thanked for constructive comments.

401 **References**


402 Buckles, L.K., Weijers, J.W.H., Verschuren, D. and Sinninghe Damsté, J.S. (2014) Sources of core and
403 intact branched tetraether membrane lipids in the lacustrine environment: Anatomy of Lake Challa and
404 its catchment, equatorial East Africa. Geochim. Cosmochim. Acta 140, 106–126,
405 https://doi.org/10.1016/j.gca.2014.04.042.

406 Dang, X., Ding, W., Yang, H., Pancost, R.D., Naafs, B.D.A., Xue, J., Xiao, L., Lu, J. and Xie, S. (2018)
407 Different temperature dependence of the bacterial brGDGT isomers in 35 Chinese lake sediments
408 compared to that in soils. Org. Geochem. 119, 72–79, https://doi.org/10.1016/j.orggeochem.2018.02.008.

409 Dang, X., Yang, H., Naafs, B.D.A., Pancost, R.D. and Xie, S. (2016a) Evidence of moisture control on
410 the methylation of branched glycerol dialkyl glycerol tetraethers in semi-arid and arid soils. Geochim.
411 Cosmochim. Acta 189, 24–36, https://doi.org/10.1016/j.gca.2016.06.004.

412 Dang, X.Y., Xue, J.T., Yang, H. and Xie, S.C. (2016b) Environmental impacts on the distribution of
413 microbial tetraether lipids in Chinese lakes with contrasting pH: Implications for lacustrine
414 paleoenvironmental reconstructions. Sci. China Earth Sci. 59, 939–950, https://doi.org/10.1007/s11430-
415 015-5234-z.

416 De Jonge, C., Hopmans, E.C., Stadnitskaia, A., Rijpstra, W.I.C., Hofland, R., Tegelaar, E. and Sinninghe
417 Damsté, J.S. (2013) Identification of novel penta- and hexamethylated branched glycerol dialkyl glycerol
418 tetraethers in peat using HPLC–$MS^2$, GC–MS and GC–SMB-MS. Org. Geochem. 54, 78–82,
419 https://doi.org/10.1016/j.orggeochem.2012.10.004.

420 De Jonge, C., Hopmans, E.C., Zell, C.I., Kim, J.-H., Schouten, S. and Sinninghe Damsté, J.S. (2014a)
421 Occurrence and abundance of 6-methyl branched glycerol dialkyl glycerol tetraethers in soils:
422 Implications for palaeoclimate reconstruction. Geochim. Cosmochim. Acta 141, 97–112,
423 https://doi.org/10.1016/j.gca.2014.06.013.

424 De Jonge, C., Stadnitskaia, A., Cherkashov, G. and Sinninghe Damsté, J.S. (2016) Branched glycerol
425 dialkyl glycerol tetraethers and crenarchaeol record post-glacial sea level rise and shift in source of
426 terrigenous brGDGTs in the Kara Sea (Arctic Ocean). Org. Geochem. 92, 42–54,
427 https://doi.org/10.1016/j.orggeochem.2015.11.009.

428 De Jonge, C., Stadnitskaia, A., Hopmans, E.C., Cherkashov, G., Fedotov, A. and Sinninghe Damsté, J.S.
429 (2014b) In situ produced branched glycerol dialkyl glycerol tetraethers in suspended particulate matter
430 from the Yenisei River, Eastern Siberia. Geochim. Cosmochim. Acta 125, 476–491,

https://doi.org/10.1016/j.gca.2013.10.031.

De Jonge, C., Stadnitskaia, A., Hopmans, E.C., Cherkashov, G., Fedotov, A., Streletskaya, I.D., Vasiliev, A.A. and Sinninghe Damsté, J.S. (2015) Drastic changes in the distribution of branched tetraether lipids in suspended matter and sediments from the Yenisei River and Kara Sea (Siberia): Implications for the use of brGDGT-based proxies in coastal marine sediments. Geochim. Cosmochim. Acta 165, 200–225, https://doi.org/10.1016/j.gca.2015.05.044.

De Rosa, M., Gambacorta, A., 1988. The lipids of archaebacteria. Prog. Lipid Res. 27, 153–175, https://doi.org/10.1016/0163-7827(88)90011-2.

Dearing Crampton-flood, E., Peterse, F., Munsterman, D. and Sinninghe Damsté, J.S. (2018) Using tetraether lipids archived in North Sea Basin sediments to extract North Western European Pliocene continental air temperatures. Earth Planet. Sci. Lett. 490, 193–205, https://doi.org/10.1016/j.epsl.2018.03.030.

Ding, S., Schwab, V.F., Ueberschaar, N., Roth, V.N., Lange, M., Xu, Y., Gleixner, G. and Pohnert, G. (2016) Identification of novel 7-methyl and cyclopentanyl branched glycerol dialkyl glycerol tetraethers in lake sediments. Org. Geochem. 102, 52–58, https://doi.org/10.1016/j.orggeochem.2016.09.009.

Ding, S., Xu, Y., Wang, Y., He, Y., Hou, J., Chen, L. and He, J.S. (2015) Distribution of branched glycerol dialkyl glycerol tetraethers in surface soils of the Qinghai–Tibetan Plateau: implications of brGDGTs-based proxies in cold and dry regions. Biogeosciences 12, 3141–3151, https://doi.org/10.5194/bg-12-3141-2015.

Freymond, C.V., Peterse, F., Fischer, L.V., Filip, F., Giosan, L. and Eglinton, T.I. (2016) Branched GDGT signals in fluvial sediments of the Danube River basin: Method comparison and longitudinal evolution. Org. Geochem. 103, 88–96, https://doi.org/10.1016/j.orggeochem.2016.11.002.

Fryer, P. (1996) Evolution of the Mariana Convergent Plate Margin System. Rev. Geophys. 34, 89–125, https://doi.org/10.1029/95RG03476.

Glud, R.N., Wenzhofer, F., Middelboe, M., Oguri, K., Turnewitsch, R., Canfield, D.E. and Kitazato, H. (2013) High rates of microbial carbon turnover in sediments in the deepest oceanic trench on Earth. Nat Geosci 6, 284–288, https://doi.org/10.1038/ngeo1773

Goñi, M.A., Monacci, N., Gisewhite, R., Ogston, A., Crockett, J. and Nittrouer, C. (2006) Distribution and sources of particulate organic matter in the water column and sediments of the Fly River Delta, Gulf of Papua (Papua New Guinea). Estuar Coast Shelf Sci 69, 225–245,

https://doi.org/10.1016/j.ecss.2006.04.012.

Guan, H., Chen, L., Luo, M., Liu, L., Mao, S., Ge, H., Zhang, M., Fang, J. and Chen, D. (2019) Composition and origin of lipid biomarkers in the surface sediments from the southern Challenger Deep, Mariana Trench. Geosci. Front. 10, 351–360, https://doi.org/10.1016/j.gsf.2018.01.004.

Herfort, L., Schouten, S., Boon, J.P., Woltering, M., Baas, M., Weijers, J.W.H. and Sinninghe Damsté, J.S. (2006) Characterization of transport and deposition of terrestrial organic matter in the southern North Sea using the BIT index. Limnol. Oceanogr. 51, 2196–2205, https://doi.org/10.4319/lo.2006.51.5.2196.

Hopmans, E.C., Schouten, S. and Sinninghe Damsté, J.S. (2016) The effect of improved chromatography on GDGT-based palaeoproxies. Org. Geochem. 93, 1–6, https://doi.org/10.1016/j.orggeochem.2015.12.006.

Hopmans, E.C., Weijers, J.W.H., Schefuss, E., Herfort, L., Sinninghe Damsté, J.S. and Schouten, S. (2004) A novel proxy for terrestrial organic matter in sediments based on branched and isoprenoid tetraether lipids. Earth Planet. Sci. Lett. 224, 107–116, https://doi.org/10.1016/j.epsl.2004.05.012.

Hu, L., Shi, X., Bai, Y., Qiao, S., Li, L., Yu, Y., Yang, G., Ma, D. and Guo, Z. (2016) Recent organic carbon sequestration in the shelf sediments of the Bohai Sea and Yellow Sea, China. J. Mar. Syst. 155, 50–58, https://doi.org/10.1016/j.jmarsys.2015.10.018.

Huguet, C., Hopmans, E.C., Feboayala, W., Thompson, D.H., Sinninghe Damsté, J.S. and Schouten, S. (2006) An improved method to determine the absolute abundance of glycerol dibiphytanyl glycerol tetraether lipids. Org. Geochem. 37, 1036–1041, https://doi.org/10.1016/j.orggeochem.2006.05.008.

Husar, R.B., Tratt, D.M., Schichtel, B.A., Falke, S.R., Li, F., Jaffe, D., Gassó, S., Gill, T., Laulainen, N.S., Lu, F., Reheis, M.C., Chun, Y., Westphal, D., Holben, B.N., Gueymard, C., McKendry, I., Kuring, N., Feldman, G.C., McClain, C., Frouin, R.J., Merrill, J., DuBois, D., Vignola, F., Murayama, T., Nickovic, S., Wilson, W.E., Sassen, K., Sugimoto, N. and Malm, W.C. (2001) Asian dust events of April 1998. J. Geophys. Res. Atmosph. 106, 18317–18330, https://doi.org/10.1029/2000JD900788.

Jamieson, A. (2015) The hadal zone: life in the deepest oceans. Cambridge University Press.

Kim, J.H., Schouten, S., Buscail, R., Ludwig, W., Bonnin, J., Sinninghe Damsté, J.S. and Bourrin, F. (2006) Origin and distribution of terrestrial organic matter in the NW Mediterranean (Gulf of Lions): Exploring the newly developed BIT index. Geochemistry Geophysics Geosystems 7, 220–222, https://doi.org/10.1029/2006GC001306.

Knappy, C.S., Nunn, C.E.M., Morgan, H.W. and Keely, B.J. (2011) The major lipid cores of the archaeon

491 Ignisphaera aggregans: implications for the phylogeny and biosynthesis of glycerol monoalkyl glycerol
492 tetraether isoprenoid lipids. Extremophiles 15, https://doi.org/10.1007/s00792-011-0382-3.
493 Lei, Y., Yang, H., Dang, X., Zhao, S. and Xie, S. (2016) Absence of a significant bias towards summer
494 temperature in branched tetraether-based paleothermometer at two soil sites with contrasting temperature
495 seasonality. Org. Geochem. 94, 83–94, https://doi.org/10.1016/j.orggeochem.2016.02.003.
496 Li, J., Naafs, B.D.A., Pancost, R.D., Yang, H., Deng, L. and Xie, S. (2017) Distribution of branched
497 tetraether lipids in ponds from Inner Mongolia, NE China: Insight into the source of brGDGTs. Org.
498 Geochem. 112, 127–136, https://doi.org/10.1016/j.orggeochem.2017.07.005.
499 Li, Y., Zhao, S., Pei, H., Shi, Q., Zang, J., Dang, X. and Yang, H. (2018) Distribution of glycerol dialkyl
500 glycerol tetraethers in surface soils along an altitudinal transect at cold and humid Mountain Changbai:
501 Implications for the reconstruction of paleoaltimetry and paleoclimate. Sci. China Earth Sci., 1–15,
502 https://doi.org/10.1007/s11430-017-9168-9.
503 Liu, J., Zheng, Y., Lin, H., Wang, X., Li, M., Liu, Y., Yu, M., Zhao, M., Pedentchouk, N., Lea-Smith,
504 D.J., Todd, J.D., Magill, C.R., Zhang, W.-J., Zhou, S., Song, D., Zhong, H., Xin, Y., Yu, M., Tian, J. and
505 Zhang, X.-H. (2019) Proliferation of hydrocarbon-degrading microbes at the bottom of the Mariana
506 Trench. Microbiome 7, https://doi.org/10.1186/s40168-019-0652-3.
507 Liu, X., Zhu, C., Wakeham, S., G and Hinrichs, K. (2014) In situ production of branched glycerol dialkyl
508 glycerol tetraethers in anoxic marine water columns. Mar Chem 166, 1–8,
509 https://doi.org/10.1016/j.marchem.2014.08.008.
510 Loomis, S.E., Russell, J.M. and Sinninghe Damsté, J.S. (2011) Distributions of branched GDGTs in soils
511 and lake sediments from western Uganda: Implications for a lacustrine paleothermometer. Org. Geochem.
512 42, 739–751, https://doi.org/10.1016/j.orggeochem.2011.06.004.
513 Luo, M., Gieskes, J., Chen, L., Shi, X. and Chen, D. (2017) Provenances, distribution, and accumulation
514 of organic matter in the southern Mariana Trench rim and slope: Implication for carbon cycle and burial
515 in hadal trenches. Mar. Geol. 386, 486–498, https://doi.org/10.1016/j.margeo.2017.02.012.
516 Martin, C., Ménot, G., Thouveny, N., Davtian, N., Andrieu-Ponel, V., Reille, M. and Bard, E. (2019)
517 Impact of human activities and vegetation changes on the tetraether sources in Lake St Front (Massif
518 Central, France). Org. Geochem. 135, 38–52, https://doi.org/10.1016/j.orggeochem.2019.06.005.
519 Meyers, P.A. (1994) Preservation of elemental and isotopic source identification of sedimentary organic
520 matter. Chem. Geol. 144, 289–302, https://doi.org/10.1016/0009-2541(94)90059-0.

521 Meyers, P.A. (1997) Organic geochemical proxies of paleoceanographic, paleolimnologic, and
522 paleoclimatic processes. Org. Geochem. 27, 213–250, httpss://doi.org/10.1016/S0146-6380(97)00049-1
523 Naafs, B.D.A., Inglis, G.N., Zheng, Y., Amesbury, M.J., Biester, H., Bindler, R., Blewett, J., Burrows,
524 M.A., Torres, D.D.C. and Chambers, F.M. (2017) Introducing global peat-specific temperature and pH
525 calibrations based on brGDGT bacterial lipids. Geochim. Cosmochim. Acta 208, 285–301,
526 https://doi.org/10.1016/j.gca.2017.01.038.
527 O'Leary, M.H. (1988) Carbon isotopes in photosynthesis. Bioscience 38, 328–336,
528 https://doi.org/10.2307/1310735
529 Peterse, F., Kim, J.-H., Schouten, S., Kristensen, D.K., Koç, N. and Sinninghe Damsté, J.S. (2009)
530 Constraints on the application of the MBT/CBT palaeothermometer at high latitude environments
531 (Svalbard, Norway). Org. Geochem. 40, 692–699, https://dx.doi.org/10.1016/j.orggeochem.2009.03.004.
532 Peterse, F., van der Meer, J., Schouten, S., Weijers, J.W.H., Fierer, N., Jackson, R.B., Kim, J.H. and
533 Sinninghe Damsté, J.S. (2012) Revised calibration of the MBT–CBT paleotemperature proxy based on
534 branched tetraether membrane lipids in surface soils. Geochim. Cosmochim. Acta 96, 215–229,
535 https://dx.doi.org/10.1016/j.gca.2012.08.011.
536 Qin, W., Carlson, L.T., Armbrust, E.V., Devol, A.H., Moffett, J.W., Stahl, D.A. and Ingalls, A.E. (2015)
537 Confounding effects of oxygen and temperature on the $TEX_{86}$ signature of marine Thaumarchaeota. Proc.
538 Natl. Acad. Sci. USA 112, https://doi.org/10.1073/pnas.1501568112.
539 Russell, J.M., Hopmans, E.C., Loomis, S.E., Liang, J. and Sinninghe Damsté, J.S. (2018) Distributions
540 of 5- and 6-methyl branched glycerol dialkyl glycerol tetraethers (brGDGTs) in East African lake
541 sediment: Effects of temperature, pH, and new lacustrine paleotemperature calibrations. Org. Geochem.
542 117, 56–69, https://doi.org/10.1016/j.orggeochem.2017.12.003.
543 Schouten, S., Hopmans, E.C., Baas, M., Boumann, H., Standfest, S., Könneke, M., Stahl, D.A. and
544 Sinninghe Damsté, J.S. (2008) Intact Membrane Lipids of "*Candidatus* Nitrosopumilus maritimus," a
545 Cultivated Representative of the Cosmopolitan Mesophilic Group I Crenarchaeota. Appl. Environ.
546 Microbiol. 74, 2433–2440, https://doi.org/10.1128/AEM.01709-07.
547 Schouten, S., Hopmans, E.C. and Sinninghe Damsté, J.S. (2013) The organic geochemistry of glycerol
548 dialkyl glycerol tetraether lipids: A review. Org. Geochem. 54, 19–61,
549 https://doi.org/10.1016/j.orggeochem.2012.09.006.
550 Sinninghe Damsté, J.S. (2016) Spatial heterogeneity of sources of branched tetraethers in shelf systems:

The geochemistry of tetraethers in the Berau River delta (Kalimantan, Indonesia). Geochim. Cosmochim. Acta 186, 13–31, https://doi.org/10.1016/j.gca.2016.04.033.

Sinninghe Damsté, J.S., Hopmans, E.C., Pancost, R.D., Schouten, S., Geenevasen, J.A.J., 2000. Newly discovered non-isoprenoid dialkyl diglycerol tetraether lipids in sediments. Chem. Commun. 23, 1683–1684, https://doi.org/10.1039/B004517I.

Sinninghe Damsté, J.S., Ossebaar, J., Abbas, B., Schouten, S. and Verschuren, D. (2009) Fluxes and distribution of tetraether lipids in an equatorial African lake: Constraints on the application of the $TEX_{86}$ palaeothermometer and BIT index in lacustrine settings. Geochim. Cosmochim. Acta 73, 4232–4249, https://doi.org/10.1016/j.gca.2009.04.022.

Sinninghe Damsté, J.S., Ossebaar, J., Schouten, S. and Verschuren, D. (2008) Altitudinal shifts in the branched tetraether lipid distribution in soil from Mt. Kilimanjaro (Tanzania): Implications for the MBT/CBT continental palaeothermometer. Org. Geochem. 39, 1072–1076, https://doi.org/10.1016/j.orggeochem.2007.11.011.

Sinninghe Damsté, J.S., Rijpstra, W.I., Hopmans, E.C., Weijers, J.W., Foesel, B.U., Overmann, J. and Dedysh, S.N. (2011) 13,16-Dimethyl octacosanedioic acid (iso-diabolic acid), a common membrane-spanning lipid of Acidobacteria subdivisions 1 and 3. Appl. Environ. Microbiol. 77, 4147–4154, https://doi.org/10.1128/aem.00466-11.

Sinninghe Damsté, J.S., Stefan, S., Hopmans, E.C., Duin, A.C.T., Van and Geenevasen, J.A.J. (2002) Crenarchaeol: the characteristic core glycerol dibiphytanyl glycerol tetraether membrane lipid of cosmopolitan pelagic crenarchaeota. J. Lipid Res. 43, 1641–1651, https://doi.org/10.1194/jlr.M200148-JLR200

Soelen, E.E.V., Kim, J.H., Santos, R.V., Dantas, E.L., Almeida, F.V.D., Pires, J.P., Roddaz, M. and Sinninghe Damsté, J.S. (2017) A 30 Ma history of the Amazon River inferred from terrigenous sediments and organic matter on the Ceará Rise. Earth Planet. Sci. Lett. 474, 40–48, https://doi.org/10.1016/j.epsl.2017.06.025.

Ta, K., Peng, X., Xu, H., Du, M., Chen, S., Li, J. and Zhang, C. (2019) Distributions and Sources of Glycerol Dialkyl Glycerol Tetraethers in Sediment Cores From the Mariana Subduction Zone. J. Geophys. Res. Biogeo. 124, 857–869, https://doi.org/10.1029/2018jg004748.

Tierney, J.E. and Russell, J.M. (2009) Distributions of branched GDGTs in a tropical lake system: Implications for lacustrine application of the MBT/CBT paleoproxy. Org. Geochem. 40, 1032–1036,

https://doi.org/10.1016/j.orggeochem.2009.04.014.

Wang, H., Liu, W. and Lu, H. (2016) Appraisal of branched glycerol dialkyl glycerol tetraether-based indices for North China. Org. Geochem. 98, 118–130, https://doi.org/10.1016/j.orggeochem.2016.05.013.

Wang, M., Zheng, Z., Zong, Y., Man, M. and Tian, L. (2019) Distributions of soil branched glycerol dialkyl glycerol tetraethers from different climate regions of China. Sci. Rep. 9 https://doi.org/10.1038/s41598-019-39147-9.

Wang, M., Zong, Y., Zheng, Z., Man, M., Hu, J. and Tian, L. (2018) Utility of brGDGTs as temperature and precipitation proxies in subtropical China. Sci. Rep. 8, https://doi.org/10.1038/s41598-41017-17964-41590

Warden, L., Kim, J.H., Zell, C., Vis, G.J., Stigter, H.D., Bonnin, J. and Sinninghe Damsté, J.S. (2016) Examining the provenance of branched GDGTs in the Tagus River drainage basin and its outflow into the Atlantic Ocean over the Holocene to determine their usefulness for paleoclimate applications. Biogeosciences 13, 5719–5738, https://doi.org/10.5194/bg-13-5719-2016.

Weber, Y., Jonge, C.D., Rijpstra, W.I.C., Hopmans, E.C., Stadnitskaia, A., Schubert, C.J., Lehmann, M.F., Sinninghe Damsté, J.S. and Niemann, H. (2015) Identification and carbon isotope composition of a novel branched GDGT isomer in lake sediments: Evidence for lacustrine branched GDGT production. Geochim. Cosmochim. Acta 154, 118–129, https://doi.org/10.1016/j.gca.2015.01.032.

Weber, Y., Sinninghe Damsté, J.S., Zopfi, J., De Jonge, C., Gilli, A., Schubert, C.J., Lepori, F., Lehmann, M.F. and Niemann, H. (2018) Redox-dependent niche differentiation provides evidence for multiple bacterial sources of glycerol tetraether lipids in lakes. Proc. Natl. Acad. Sci. USA 115, 10926, https://doi.org/10.1073/pnas.1805186115.

Weijers, J.W.H., Schefuß, E., Kim, J.-H., Sinninghe Damsté, J.S. and Schouten, S. (2014) Constraints on the sources of branched tetraether membrane lipids in distal marine sediments. Org. Geochem. 72, 14–22, https://doi.org/10.1016/j.orggeochem.2014.04.011.

Weijers, J.W.H., Schouten, S., Donker, J.C.V.D., Hopmans, E.C. and Sinninghe Damsté, J.S. (2007a) Environmental controls on bacterial tetraether membrane lipid distribution in soils. Geochim. Cosmochim. Acta 71, 703–713, https://doi.org/10.1016/j.gca.2006.10.003.

Weijers, J.W.H., Schefuß, E., Schouten, S. and Sinninghe Damsté, J.S. (2007b) Coupled thermal and hydrological evolution of tropical Africa over the last deglaciation. Science 315, 1701–1704, https://doi.org/10.1126/science.1138131.

611 Wu, W., Zhao, L., Pei, Y., Ding, W., Yang, H. and Xu, Y. (2013) Variability of tetraether lipids in Yellow
612 River-dominated continental margin during the past eight decades: Implications for organic matter
613 sources and river channel shifts. Org. Geochem. 60, 33–39,
614 https://doi.org/10.1016/j.orggeochem.2013.04.014.
615 Xiao, W., Wang, Y., Zhou, S., Hu, L., Yang, H. and Xu, Y. (2016) Ubiquitous production of branched
616 glycerol dialkyl glycerol tetraethers (brGDGTs) in global marine environments: A new source indicator
617 for brGDGTs. Biogeosciences 13, 5883–5894, https://doi.org/10.5194/bg-13-5883-2016.
618 Xiao, W., Wang, Y., Liu, Y., Zhang, X., Shi, L., Fang, J. and Xu, Y. (2019) Predominance of
619 hexamethylated 6-methyl branched glycerol dialkyl glycerol tetraethers in the Mariana Trench: Source
620 and environmental implication. Figshare, https://doi.org/10.6084/m9.figshare.9896120.v1.
621 Xiao, W., Xu, Y., Ding, S., Wang, Y., Zhang, X., Yang, H., Wang, G. and Hou, J. (2015) Global calibration
622 of a novel, branched GDGT-based soil pH proxy. Org. Geochem. 89–90, 56–60,
623 https://doi.org/10.1016/j.orggeochem.2015.10.005.
624 Xie, S., Liu, X.L., Schubotz, F., Wakeham, S.G. and Hinrichs, K.U. (2014) Distribution of glycerol ether
625 lipids in the oxygen minimum zone of the Eastern Tropical North Pacific Ocean. Org. Geochem. 71, 60–
626 71, https://doi.org/10.1016/j.orggeochem.2014.04.006.
627 Xu, Y., Ge, H. and Fang, J. (2018) Biogeochemistry of hadal trenches: Recent developments and future
628 perspectives. Deep Sea Res. Part II Top. Stud. Oceanogr. 155, 19–26,
629 https://doi.org/10.1016/j.dsr2.2018.10.006.
630 Yang, H., Lü, X., Ding, W., Lei, Y., Dang, X. and Xie, S. (2015) The 6-methyl branched tetraethers
631 significantly affect the performance of the methylation index (MBT') in soils from an altitudinal transect
632 at Mount Shennongjia. Org. Geochem. 82, 42–53, https://doi.org/10.1016/j.orggeochem.2015.02.003.
633 Yang, H., Pancost, R.D., Dang, X., Zhou, X., Evershed, R.P., Xiao, G., Tang, C., Gao, L., Guo, Z. and
634 Xie, S. (2014) Correlations between microbial tetraether lipids and environmental variables in Chinese
635 soils: Optimizing the paleo-reconstructions in semi-arid and arid regions. Geochim. Cosmochim. Acta
636 126, 49–69, https://doi.org/10.1016/j.gca.2013.10.041.
637 Zang, J., Lei, Y. and Yang, H. (2018) Distribution of glycerol ethers in Turpan soils: implications for use
638 of GDGT-based proxies in hot and dry regions. Front. Earth Sci., https://doi.org/10.1007/s11707-11018-
639 10722-z.
640 Zell, C., Kim, J.-H., Moreira-Turcq, P., Abril, G., Hopmans, E.C., Bonnet, M.-P., Sobrinho, R.L. and

641 Sinninghe Damsté, J.S. (2013) Disentangling the origins of branched tetraether lipids and crenarchaeol
642 in the lower Amazon River: Implications for GDGT-based proxies. Limnol. Oceanogr. 58, 343–353,
643 https://doi.org/10.4319/lo.2013.58.1.0343.
644 Zell, C., Kim, J.H., Balsinha, M., Dorhout, D., Fernandes, C., Baas, M. and Sinninghe Damsté, J.S.
645 (2014a) Transport of branched tetraether lipids from the Tagus River basin to the coastal ocean of the
646 Portuguese margin: consequences for the interpretation of the MBT'/CBT paleothermometer.
647 Biogeosciences 11, 5637–5655, https://doi.org/10.5194/bg-11-5637-2014.
648 Zell, C., Kim, J.H., Hollander, D., Lorenzoni, L., Baker, P., Silva, C.G., Nittrouer, C. and Sinninghe
649 Damsté, J.S. (2014b) Sources and distributions of branched and isoprenoid tetraether lipids on the
650 Amazon shelf and fan: Implications for the use of GDGT-based proxies in marine sediments. Geochim.
651 Cosmochim. Acta 139, 293–312, https://doi.org/10.1016/j.gca.2014.04.038.
652 Zeng, Z., Liu, X.-L., Farley, K.R., Wei, J.H., Metcalf, W.W., Summons, R.E. and Welander, P.V. (2019)
653 GDGT cyclization proteins identify the dominant archaeal sources of tetraether lipids in the ocean. Proc.
654 Natl. Acad. Sci. USA 116, 22505, https://doi.org/10.1073/pnas.1909306116.
655 Zhang, C., Wang, J., Wei, Y., Zhu, C., Huang, L. and Dong, H. (2012) Production of branched tetraether
656 lipids in the lower Pearl River and estuary: effects of extraction methods and impact on bGDGT proxies.
657 Front. Microbiol. 2 https://doi.org/10.3389/fmicb.2011.00274.
658 Zhu, C., Weijers, J.W.H., Wagner, T., Pan, J.M., Chen, J.F. and Pancost, R.D. (2011) Sources and
659 distributions of tetraether lipids in surface sediments across a large river-dominated continental margin.
660 Org. Geochem. 42, 376–386, https://doi.org/10.1016/j.orggeochem.2011.02.002.
661
662

663 **Figure and Table captions**

664 **Table 1.** Organic carbon (OC) content, total nitrogen (TN) content, molar ratio of OC/TN and stable
665 carbon isotopic composition ($\delta^{13}C_{OC}$) in the Mariana Trench sediments

666 **Table 2.** Fractional abundance and concentration of brGDGTs and iGDGT in the Mariana Trench
667 sediments.

668 **Figure 1.** Location of the samples in this study. Red, orange, gray, blue and purple circles indicate
669 globally distributed soil, river, lake, peat and marine samples, respectively. Black star denotes the
670 sediment core in the Mariana Trench. The detailed information is provided in supplementary
671 material.

672 **Figure 2.** Chemical structures of brGDGTs and crenarchaeol.

673 **Figure 3.** Extracted ion chromatograms (EICs) of *m/z* 1050 (left) and *m/z* 1036 (right) showing
674 separation of 5-methyl and 6-methyl brGDGTs in soil (top), Mariana Trench sediment (middle) and
675 combined soil and sediment (bottom).

676 **Figure 4.** Plot of $\delta^{13}C_{OC}$ versus TN/OC for core sediments from the Mariana Trench (MT). Included
677 in this graph are different compositional ranges of $C_3$ vascular plants, $C_4$ vascular plants, bacteria,
678 river and estuary phytoplankton and marine phytoplankton sources. The compositional range of
679 different end members was cited from Goñi et al. (2006) and Hu et al. (2016). The red stars and
680 green stars denote data from this study and Luo et al. (2017) respectively.

681 **Figure 5.** Comparisons of distribution of 15 brGDGT compounds in soil (n = 634), peat (n = 473),
682 river (n = 88), lake (n = 410), marine (n = 415) and Mariana Trench (n = 11) samples.

683 **Figure 6.** Relationship between the (IIIa + IIIa')/(IIa + IIa') index and the BIT index of the Mariana
684 Trench sediments (star) and globally distribute soil (circle) and marine samples (square). The dashed
685 lines represent the upper limit of production in the terrestrial realm and the lower limit of production
686 in the marine realm defined by Xiao et al. (2016).

687 **Figure 7.** Vertical profiles of a) the proportion of GDGT-IIIa', b) $\delta^{13}C_{OC}$ and c) BIT index of a
688 marine sediment core from the North Sea Basin (Dearing Crampton-flood et al., 2018). Vertical
689 profiles of d) the proportion of GDGT-IIIa', e) $\delta^{13}C_{OC}$, f) BIT index of a marine sediment core from
690 the Kara Sea (De Jonge et al., 2016). Spatial distribution patterns of g) average distribution of
691 brGDGTs and h) BIT index in the transect from the land to the ocean off the Portuguese coast (river

floodplain, mudbelt, Lisbon canyon head and lower Setúbal canyon) (Warden et al., 2016). Isosurface plots of i) BIT index, j) $\delta^{13}C_{OC}$ and k) the proportion of GDGT-IIIa' of the surface sediments from the Berau River delta (Sinninghe Damsté, 2016).

**Figure 8** Ternary diagram showing the fractional abundances of tetra-, penta- and hexamethylated brGDGTs. The compiled dataset includes globally distributed soil, peat, lake, river and marine samples, as well as the Mariana Trench sediments.

**Figure 9** Scatterplots of the (IIIa + IIIa')/(IIa + IIa') ratio versus the proportion of brGDGT-IIIa' in globally distributed soils and marine sediments. The solid, dashed and dotted line denotes the Linear fit, 95% confidence band and 95% prediction band of concatenated data, respectively. The number of samples, slope, $R^2$ and *p* values of calibration are for the global distributed soils, marine sediments and Mariana Trench sediments.

**Table 1.** Organic carbon (OC) content, total nitrogen (TN) content, molar ratio of OC/TN and stable carbon isotopic composition ($\delta^{13}C_{OC}$) in the Mariana Trench sediments

| Sample ID | Depth (cm) | OC (wt. %) | TN (wt. %) | OC/TN (mol/mol) | $\delta^{13}C_{OC}$ (‰) |
|---|---|---|---|---|---|
| MT1 | 0-2 | 0.31 | 0.05 | 6.52 | –20.02 |
| MT2.5 | 2-3 | 0.27 | 0.05 | 6.05 | –19.66 |
| MT3.5 | 3-4 | 0.29 | 0.05 | 6.85 | –19.55 |
| MT4.5 | 4-5 | 0.27 | 0.05 | 5.78 | –19.84 |
| MT5.5 | 5-6 | 0.29 | 0.06 | 6.13 | –19.94 |
| MT6.5 | 6-7 | 0.30 | 0.06 | 5.62 | –19.47 |
| MT7.5 | 7-8 | 0.27 | 0.04 | 7.27 | -19.54 |
| MT8.5 | 8-9 | 0.29 | 0.05 | 6.93 | –19.82 |
| MT9.5 | 9-10 | 0.28 | 0.04 | 7.74 | –20.09 |
| MT10.5 | 10-11 | 0.26 | 0.04 | 8.34 | –20.27 |

**Table 2.** Fractional abundance of brGDGTs and iGDGTs in the Mariana Trench sediments.

| Sample ID | Ia (%) | Ib (%) | Ic (%) | IIa (%) | IIa' (%) | IIb (%) | IIb' (%) | IIc (%) | IIc' (%) | IIIa (%) | IIIa' (%) | IIIb (%) | IIIb' (%) | IIIc (%) | IIIc' (%) | brGDGTs (%) | iGDGTs (%) |
|---|---|---|---|---|---|---|---|---|---|---|---|---|---|---|---|---|---|
| MT1 | 13.6 | 2.7 | 1.5 | 0.0 | 10.4 | 0.0 | 0.0 | 0.0 | 0.0 | 0.0 | 71.8 | 0.0 | 0.0 | 0.0 | 0.0 | 3.2 | 96.8 |
| MT2.5 | 13.5 | 2.4 | 1.6 | 0.0 | 12.1 | 0.0 | 1.3 | 0.0 | 0.0 | 0.0 | 69.0 | 0.0 | 0.0 | 0.0 | 0.0 | 2.0 | 98.0 |
| MT3.5 | 11.1 | 1.4 | 0.6 | 0.0 | 9.5 | 0.0 | 0.6 | 0.0 | 0.0 | 0.0 | 76.2 | 0.0 | 0.6 | 0.0 | 0.0 | 1.5 | 98.5 |
| MT4.5 | 14.2 | 1.4 | 0.9 | 0.0 | 9.2 | 0.0 | 0.4 | 0.0 | 0.0 | 0.0 | 73.9 | 0.0 | 0.0 | 0.0 | 0.0 | 1.5 | 98.5 |
| MT5.5 | 11.1 | 2.0 | 0.8 | 0.0 | 10.3 | 0.0 | 0.8 | 0.0 | 0.0 | 0.0 | 75.0 | 0.0 | 0.0 | 0.0 | 0.0 | 1.5 | 98.5 |
| MT6.5 | 11.2 | 2.1 | 0.9 | 0.0 | 9.1 | 0.0 | 0.0 | 0.0 | 0.0 | 0.0 | 76.0 | 0.0 | 0.8 | 0.0 | 0.0 | 1.7 | 98.3 |
| MT7.5 | 13.4 | 1.5 | 1.0 | 0.0 | 11.3 | 0.0 | 1.2 | 0.0 | 0.0 | 0.0 | 71.5 | 0.0 | 0.0 | 0.0 | 0.0 | 1.4 | 98.6 |
| MT8.5 | 13.0 | 2.2 | 1.1 | 0.0 | 12.7 | 0.0 | 0.0 | 0.0 | 0.0 | 0.0 | 70.9 | 0.0 | 0.0 | 0.0 | 0.0 | 1.4 | 98.6 |
| MT9.5 | 11.8 | 2.0 | 0.7 | 0.0 | 9.2 | 0.0 | 0.0 | 0.0 | 0.0 | 0.0 | 76.3 | 0.0 | 0.0 | 0.0 | 0.0 | 1.7 | 98.3 |
| MT10.5 | 11.8 | 1.8 | 1.0 | 0.0 | 10.6 | 0.0 | 1.0 | 0.0 | 0.4 | 0.0 | 73.3 | 0.0 | 0.0 | 0.0 | 0.0 | 1.7 | 98.3 |

**Figure 1.** Location of the samples in this study. Red, orange, gray, blue and purple circles indicate globally distributed soil, river, lake, peat and marine samples, respectively. Black star denotes the sediment core in the Mariana Trench. The detailed information is provided in supplementary material.

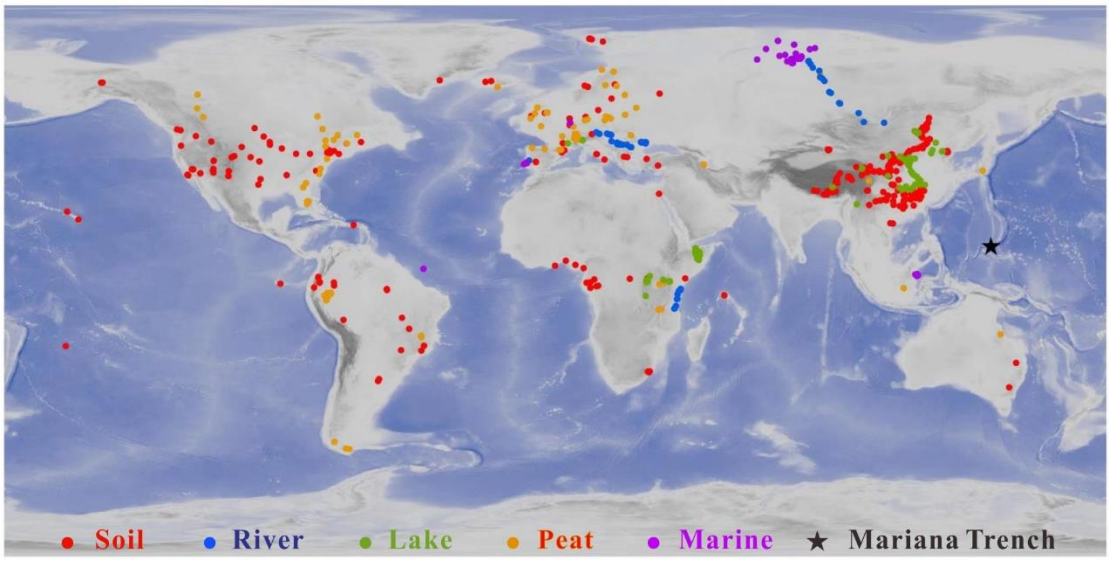

**Figure 2.** Chemical structures of brGDGTs and crenarchaeol.

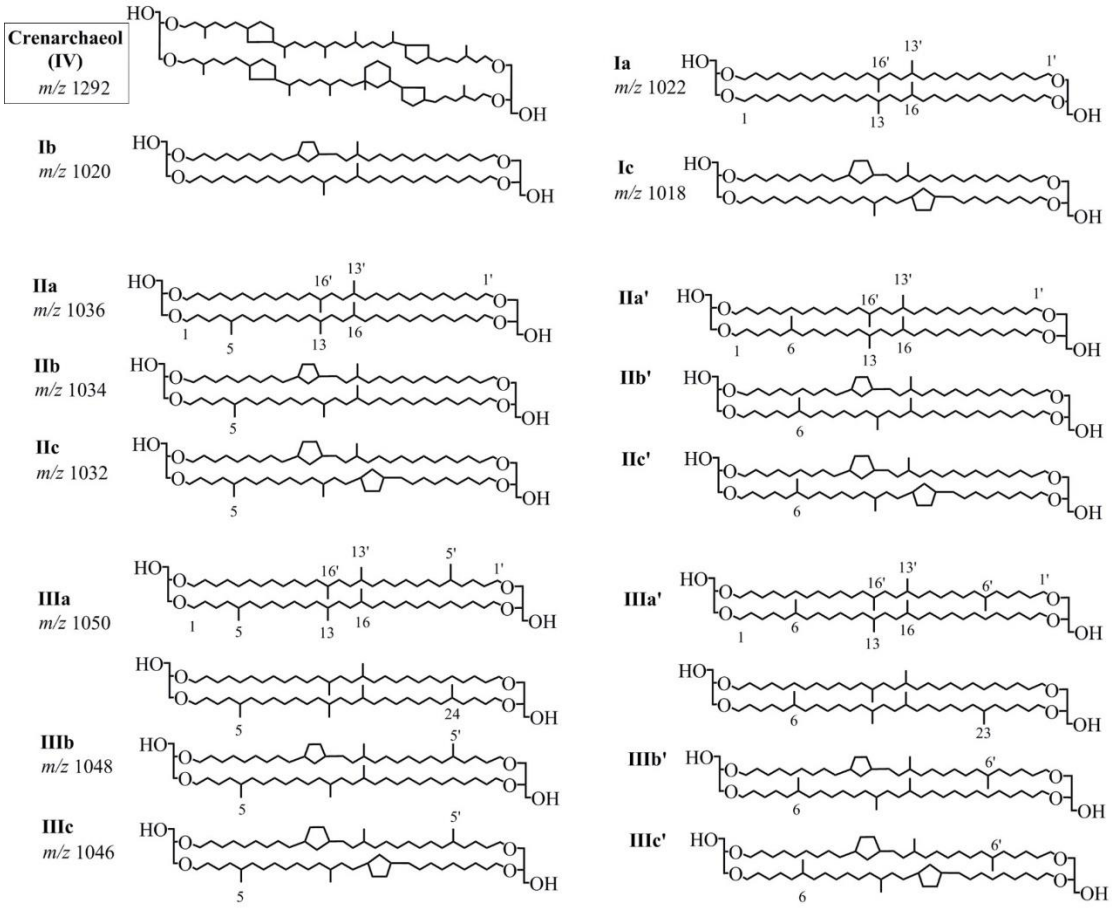

**Figure 3.** Extracted ion chromatograms (EICs) of *m/z* 1050 (left) and *m/z* 1036 (right) showing separation of 5-methyl and 6-methyl brGDGTs in soil (top), Mariana Trench sediment (middle) and combined soil and sediment (bottom).

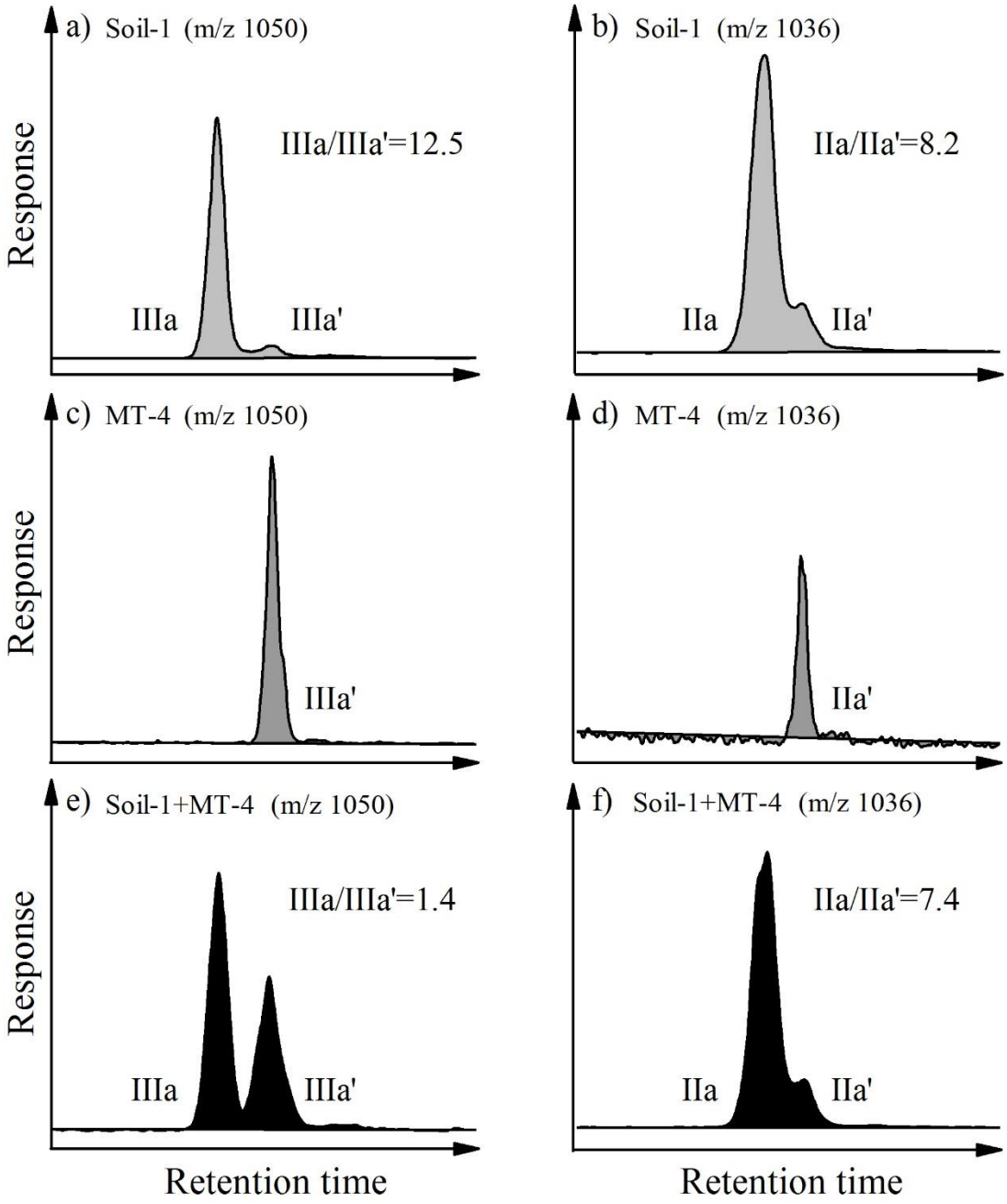

**Figure 4.** Plot of $\delta^{13}C_{OC}$ versus TN/OC for core sediments from the Mariana Trench (MT). Included in this graph are different compositional ranges of $C_3$ vascular plants, $C_4$ vascular plants, bacteria, river and estuary phytoplankton and marine phytoplankton sources. The compositional range of different end members was cited from Goñi et al. (2006) and Hu et al. (2016). The red stars and green stars denote data from this study and Luo et al. (2017) respectively.

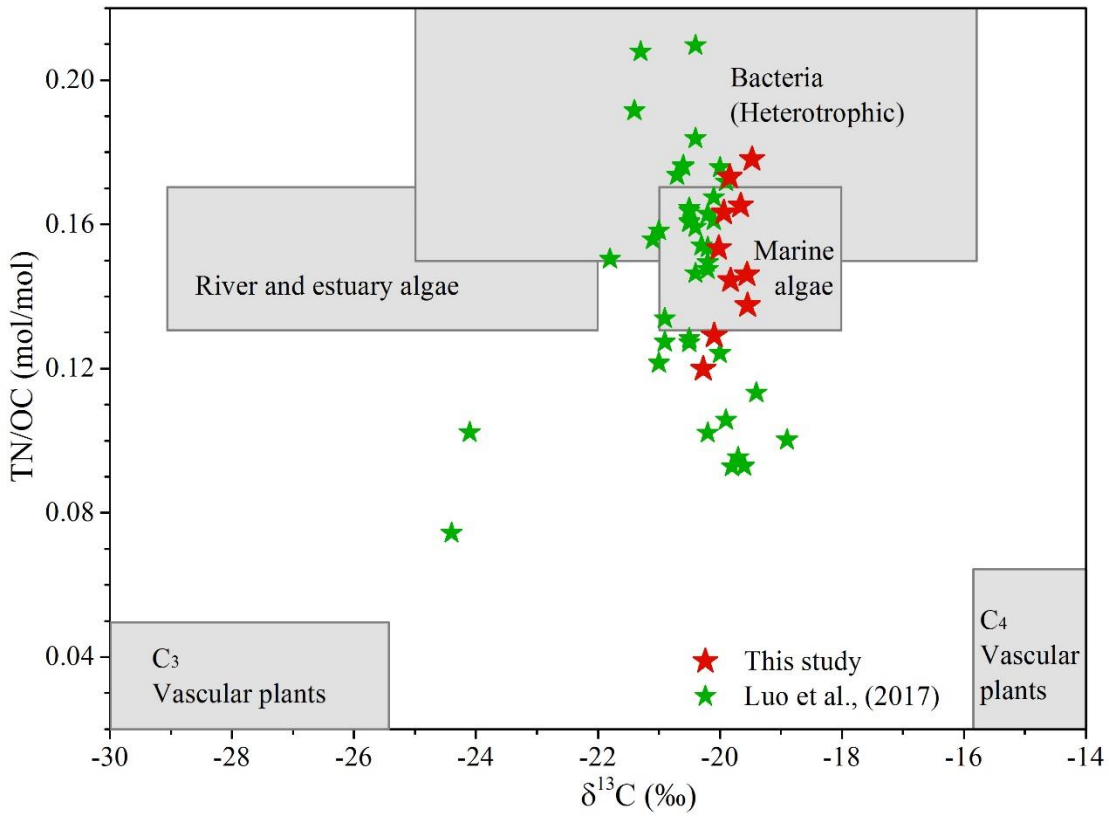

**Figure 5.** Comparisons of distribution of 15 brGDGT compounds in soil (n = 634), peat (n = 473), river (n = 88), lake (n = 410), marine (n = 415) and Mariana Trench (n = 11) samples.

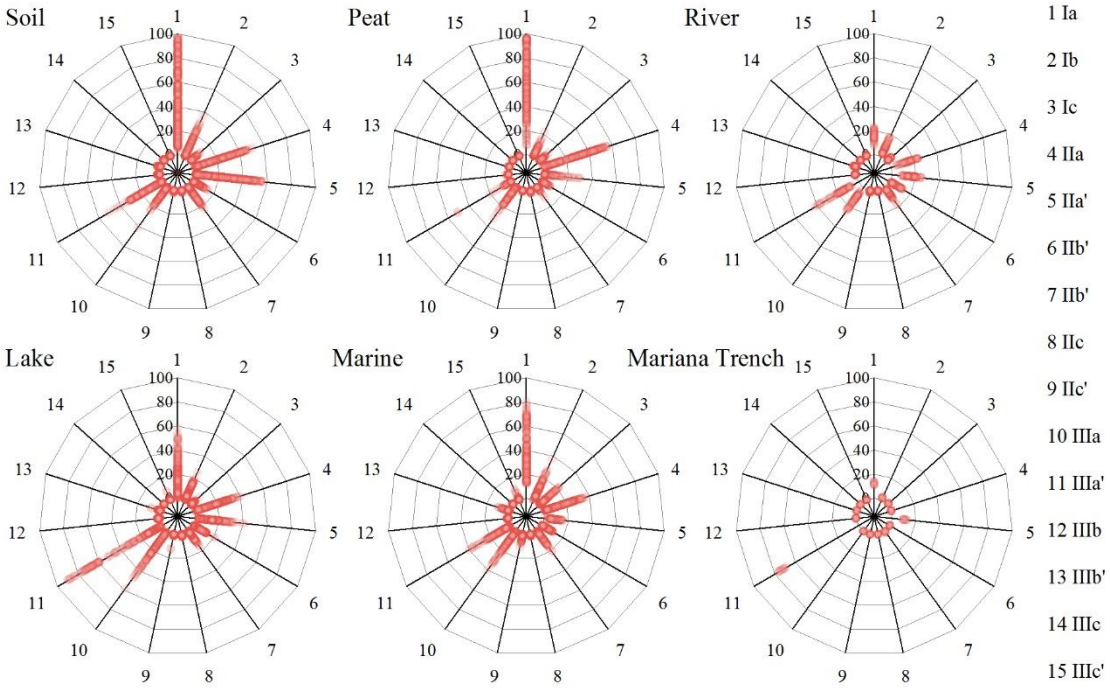

**Figure 6.** Relationship between the (IIIa + IIIa')/(IIa + IIa') index and the BIT index of the Mariana Trench sediments (star) and globally distribute soil (circle) and marine samples (square). The dashed lines represent the upper limit of production in the terrestrial realm and the lower limit of production in the marine realm defined by Xiao et al. (2016).

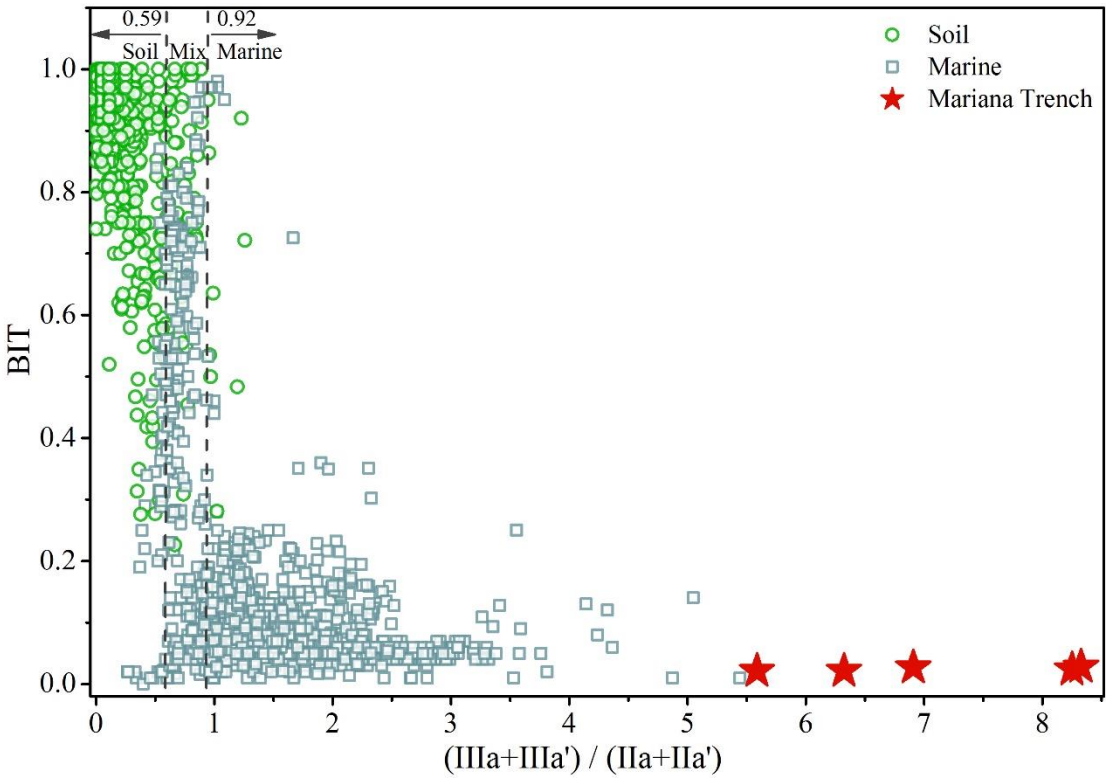

**Figure 7.** Vertical profiles of a) the proportion of GDGT-IIIa', b) $\delta^{13}C_{OC}$ and c) BIT index of a marine sediment core from the North Sea Basin (Dearing Crampton-flood et al., 2018). Vertical profiles of d) the proportion of GDGT-IIIa', e) $\delta^{13}C_{OC}$, f) BIT index of a marine sediment core from the Kara Sea (De Jonge et al., 2016). Spatial distribution patterns of g) average distribution of brGDGTs and h) BIT index in the transect from the land to the ocean off the Portuguese coast (river floodplain, mudbelt, Lisbon canyon head and lower Setúbal canyon) (Warden et al., 2016). Isosurface plots of i) BIT index, j) $\delta^{13}C_{OC}$ and k) the proportion of GDGT-IIIa' of the surface sediments from the Berau River delta (Sinninghe Damsté, 2016).

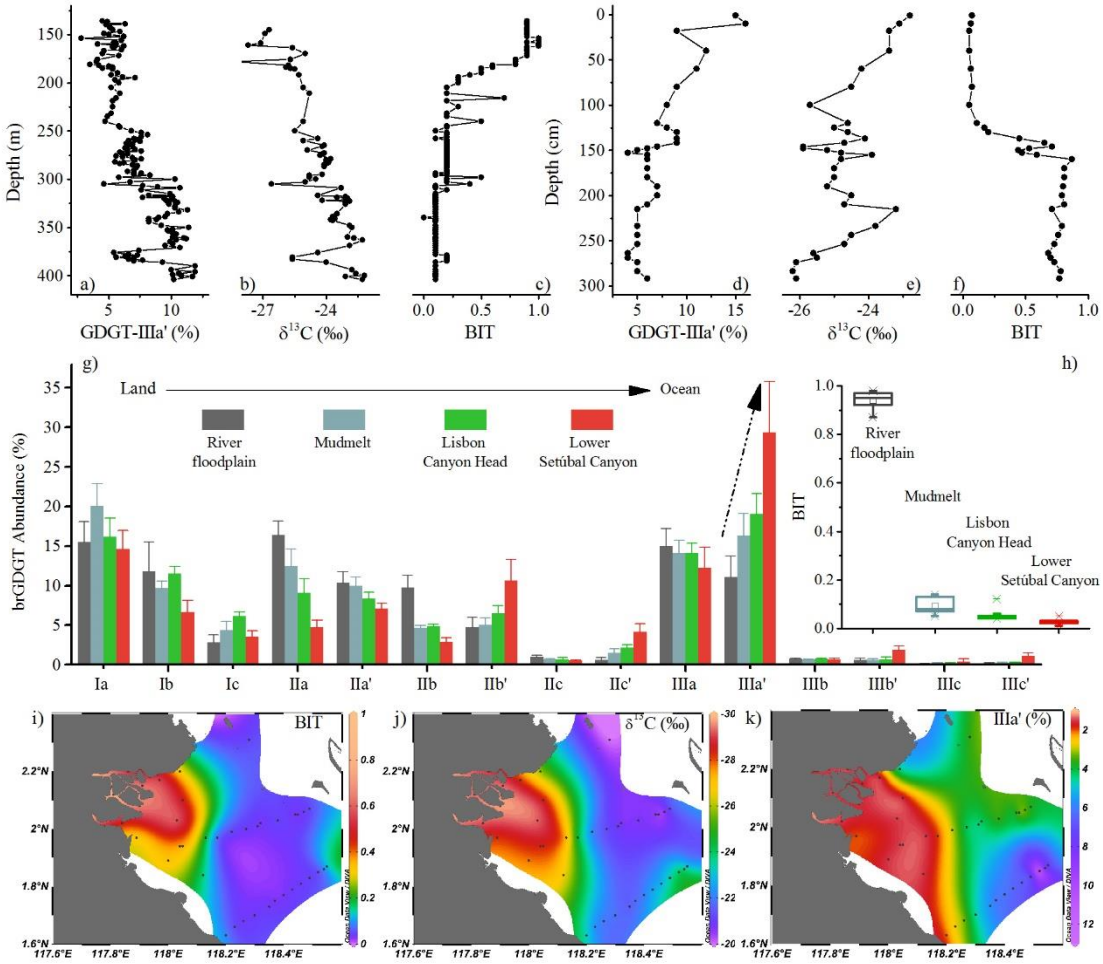

**Figure 8** Ternary diagram showing the fractional abundances of tetra-, penta- and hexamethylated brGDGTs. The compiled dataset includes globally distributed soil, peat, lake, river and marine samples, as well as the Mariana Trench sediments.

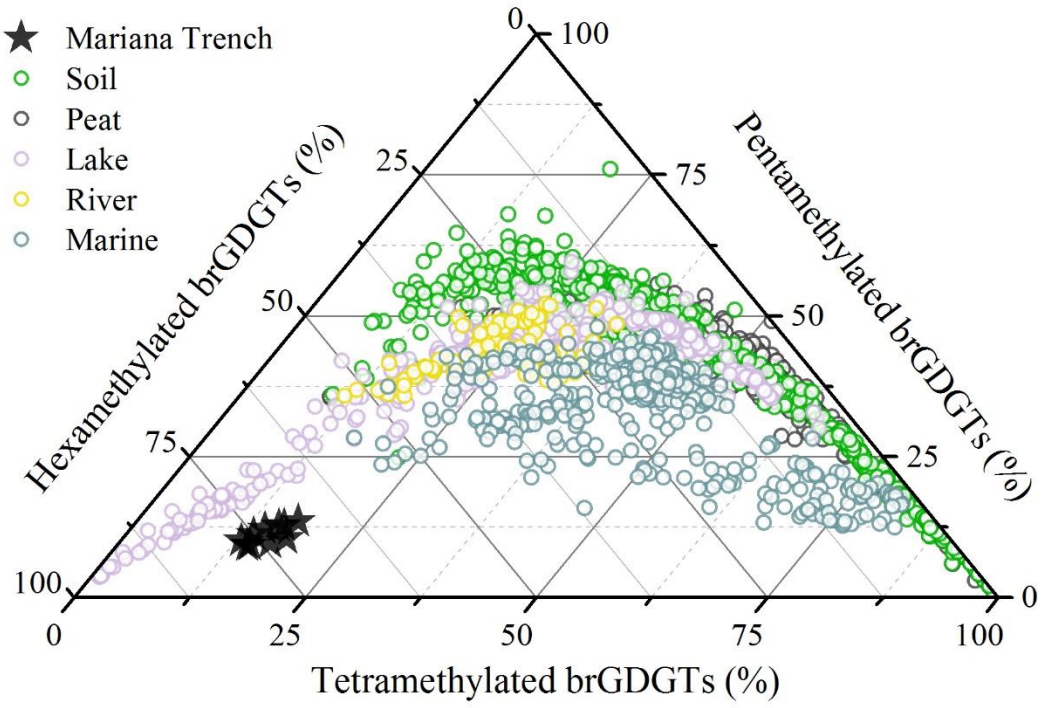

**Figure 9** Scatterplots of the (IIIa + IIIa')/(IIa + IIa') ratio versus the proportion of brGDGT-IIIa' in globally distributed soils and marine sediments. The solid, dashed and dotted line denotes the Linear fit, 95% confidence band and 95% prediction band of concatenated data, respectively. The number of samples, slope, $R^2$ and *p* values of calibration are for the global distributed soils, marine sediments and Mariana Trench sediments.